A Generalized Equivalent Circuit Applied to a Tunable Sapphire-Loaded Superconducting Cavity

Michael E. Tobar, *Student Member, IEEE*, and David G. Blair

Abstract—**A Lagrangian technique is used to develop an equivalent circuit for a loop-coupled tunable sapphire-loaded superconducting cavity resonator (T-SLOSC) by considering separately the sapphire dielectric and the cavity. Interaction between modes during tuning is characterized by cross coupling components between equivalent mode circuits. Cross-coupling coefficients are defined with respect to the fields in the resonator and equivalent circuit components. Coupling between modal fields is shown to be predominantly reactive in the sapphire-loaded cavity, and can degrade a mode with $Q > 10^8$ by a few orders of magnitude. Interactions between line resonances and T-SLOSC modes are observed to be predominantly resistive through the superconducting niobium probes. Cross-coupling coefficients between some interacting modes have been determined and the reflection coefficients modeled.**

I. Introduction

THE tunable sapphire-loaded superconducting cavity resonator (T-SLOSC) under investigation is being developed as a dielectric resonator in an ultra-low-phase-noise, tunable, cryogenic, X-band loop oscillator. Its use is in a parametric transducer system for a resonant bar gravitational wave antenna at the University of Western Australia [1]. Similar devices could be used for any application requiring low-phase-noise X-band signal sources.

Fixed-frequency [2], [3] and tunable [4] sapphire resonators have been described previously. These resonators exploit the low loss tangent of sapphire at cryogenic temperatures, with achievable Q values greater than 10^9. However, the permittivity of sapphire is only about 10, so to obtain confinement of about 95% in the sapphire part of the loaded cavity, a high circumferential mode number is required. The two modes analysed in this paper have been identified to have circumferential mode numbers of 6 and 8 [5]. Thus the cavity is overmoded, and when tuning the desired operational mode, other modes can tune near and interact with this operational mode.

Manuscript received August 3, 1990. This work was done as part of the Gravitational Radiation Detection Project at the University of Western Australia. It was supported by the Australian Research Council.

The authors are with the Physics Department, University of Western Australia, Nedlands 6009, W.A., Australia.

IEEE Log Number 9101123.

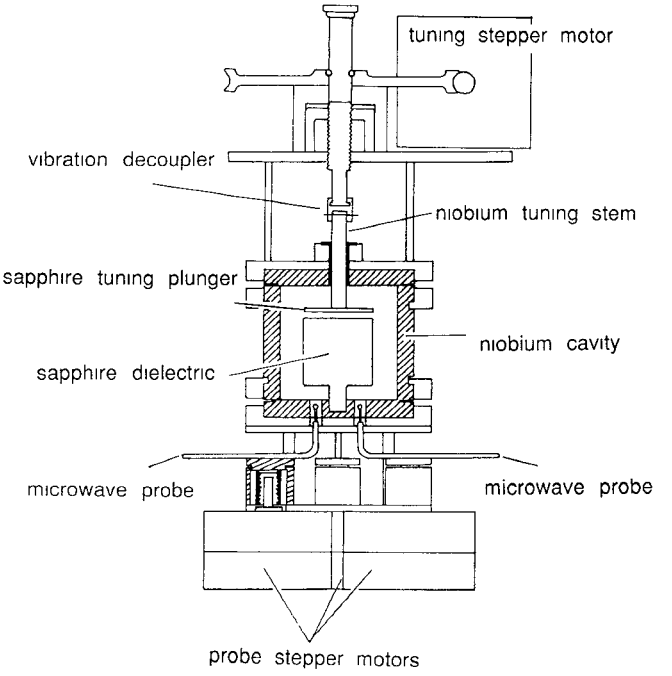

Fig. 1. Scale diagram of the construction of the T-SLOSC, where the internal dimension of the nobium cavity is 50×50 mm.

Construction is illustrated in Fig. 1. The resonant sapphire cylindrical mushroom height by diameter dimension is 27.5×30.1 mm, while the sapphire tuning disk is 3×30.1 mm. Both are inside a 50×50 mm cylindrical niobium cavity. The sapphire tuning disk affects the evanescent field outside the sapphire and perturbs the resonant frequency. Tuning is achieved by the tuning stepper motor; typically a tuning range of the order of tens of MHz is achieved for a mode with an unloaded Q of a few hundred million. Three niobium probes couple to and extract electromagnetic energy within the cavity. The probe stepper motors vary the coupling to particular modes.

For high-Q modes only approximately half a percent tuning of eigenfrequencies is experienced. Therefore eigenfunction field patterns experience only small field perturbations. One might thus expect the quality factor to

0018-9480/91/0900-1582$01.00 ©1991 IEEE

remain high throughout the tuning range. This is desirable in that the phase noise obtainable from the constructed loop oscillator is dependent on this high quality factor. Experimental results reveal that while tuning, modes interact. If a high-Q mode interacts with a low-Q mode, the high-Q mode will experience a severe drop in Q.

Complete field solutions of coupled cavities are very difficult. However a cavity coupling system may be replaced by impedance or admittance elements of known magnitude and frequency dependence. For a right cylindrical resonator an equivalent circuit based on a Lagrangian technique [6] has been used to derive equivalent circuit parameters from known field patterns and cavity properties. In a fixed right cylinder there are no interactions between modes; i.e., the associated eigenfunction field patterns are orthogonal. In this case cross couplings between modes are nonexistent. Previous work [7] has shown that a mutual resistive interaction was apparent in a tunable echo box between degenerate modes. This also occurs in the T-SLOSC when modes interact with line resonances. However, for modal interactions a mutual reactive effect dominates as a consequence of the reactive sapphire dielectric. This type of effect has been observed previously between two similar sapphire disk resonators [8].

All internal elements add possibilities for mutual interactions. We have generalized previous theory [6], [7], [9] to include all possible mutual interacting terms. This keeps Lagrange's equations and the equivalent circuit representation as general as possible. These interacting modes have been modeled on Mathematica [10]. Results show the Q degradation observed for reactive coupling between modes. Resistive interaction modeling reveals that a higher Q mode distorts as it tunes across the bandwidth of a lower Q mode. In our experiments this effect was apparent across line resonances.

This paper describes high-precision measurements of mode interactions made possible by the use of an ultrastable sapphire-loaded superconducting cavity (SLOSC) oscillator within a theoretical framework for understanding the observed behavior. A general expression for the reflection coefficient of two interacting modes is derived. Taking a very precise look at some reactively and resistively coupled interactions experimentally verifies the generalized reflection coefficient derived.

II. Equivalent Circuit—Theoretical Development

Separating the sapphire dielectric and niobium cavity parts, the loop-coupled Lagrangian equations for a given mode n will be presented. Either q_n (electric charge) or ϕ_n (magnetic flux) are chosen as normal coordinates, corresponding to a resonant wavenumber k_n. Duality exists between these electric and magnetic quantities, and it is assumed that the electromagnetic field in the cavity and sapphire can be expanded in terms of the normal coordinates $\phi_n, \dot{\phi}_n$ or $q_n, \dot{q}_n$ respectively, with eigenvalues k_n and dimensionless vector eigenfunctions $\boldsymbol{\xi}_n, \boldsymbol{\eta}_n$. Thus,

$$\boldsymbol{H} = \sum_n k_n \dot{q}_n \boldsymbol{\eta}_n \tag{1a}$$

$$\boldsymbol{D} = \sum_n k_n^2 q_n \boldsymbol{\xi}_n \tag{1b}$$

in the cavity or

$$\boldsymbol{B} = \sum_n k_n^2 \phi_n \boldsymbol{\eta}_n \tag{2a}$$

$$\boldsymbol{E} = \sum_n k_n \dot{\phi}_n \boldsymbol{\xi}_n \tag{2b}$$

in the sapphire.

The dimensionless vector eigenfunctions obey the wave equations:

$$\nabla^2 \boldsymbol{\xi}_n + k_n^2 \boldsymbol{\xi}_n = 0 \qquad \nabla \cdot \boldsymbol{\xi}_n = 0 \tag{3a}$$

$$\nabla^2 \boldsymbol{\eta}_n + k_n^2 \boldsymbol{\eta}_n = 0 \qquad \nabla \cdot \boldsymbol{\eta}_n = 0 \tag{3b}$$

and relevant boundary conditions on the sapphire dielectric or superconducting cavity walls. If no coupling between modes occurs, the following orthogonality conditions hold true:

$$\int_{\text{dielectric volume}} \boldsymbol{\xi}_n \cdot \boldsymbol{\xi}_m \, dt = \delta_{nm} v_d \tag{4a}$$

$$\int_{\text{dielectric volume}} \boldsymbol{\eta}_n \cdot \boldsymbol{\eta}_m \, dt = \delta_{nm} v_d \tag{4b}$$

$$\int_{\text{cavity volume}} \boldsymbol{\xi}_n \cdot \boldsymbol{\xi}_m \, dt = \delta_{nm} v_c \tag{5a}$$

$$\int_{\text{cavity volume}} \boldsymbol{\eta}_n \cdot \boldsymbol{\eta}_m \, dt = \delta_{nm} v_c. \tag{5b}$$

Here v_d and v_c are the dielectric and cavity volume respectively and δ_{nm} is the Kroneker delta. Also $\boldsymbol{\xi}_n$ and $\boldsymbol{\eta}_n$ are related by

$$k_n \boldsymbol{\xi}_n = \nabla \times \boldsymbol{\eta}_n \qquad -k_n \boldsymbol{\eta}_n = \nabla \times \boldsymbol{\xi}_n. \tag{6}$$

Using the electric current coordinates q_n and $\dot{q}_n$, a series circuit naturally evolves from the theory. Modeling the cavity, the series loss represents the surface resistance losses of the niobium superconductor. Using the magnetic flux coordinates ϕ_n and $\dot{\phi}_n$, a parallel circuit naturally evolves from the theory. Modeling the sapphire, the dissipative term represents a shunt dielectric loss. The series circuit can be transformed to a parallel circuit for a general mode with $Q \gg 1$ [6], and vice versa. This dual representation can be taken further when regarding interactions between modes by introducing cross-coupling terms. When attempting to isolate these parameters to either superconducting niobium or sapphire dielectric, both representations are needed to understand meaningful equivalent circuit parameters in terms of the modal fields.

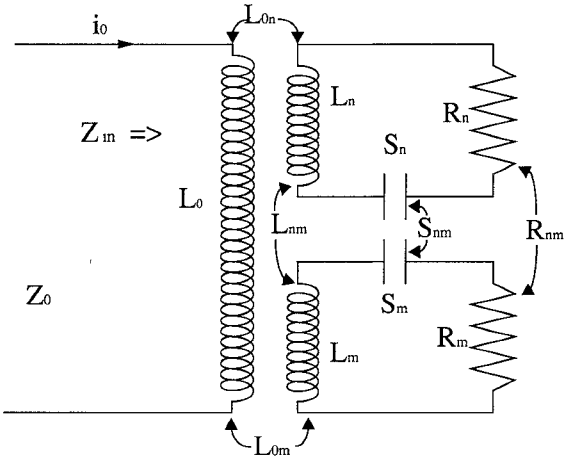

Fig. 2. General equivalent circuit of two excited modes in a loop-coupled cavity as derived from normal coordinates q_n and q_m.

A. Series Circuit Representation of the Niobium Cavity

In this subsection we shall derive the series equivalent circuit of Fig. 2 with respect to the electric charge coordinates q_n and q_m. Assuming only two excited modes, n and m, and using (1a) and (1b), the magnetic and electric field energies in the cavity can be represented by the respective Lagrangian variables:

$$T_{nm} = \frac{\mu}{2}\int_{\text{cavity volume}} \boldsymbol{H}_n \cdot \boldsymbol{H}_m \, d\tau$$

$$= \frac{\mu k_n k_m \dot{q}_n \dot{q}_m}{2}\int_{\text{cavity}} \boldsymbol{\eta}_n \cdot \boldsymbol{\eta}_m \, d\tau \tag{7}$$

$$V_{nm} = \frac{1}{2\epsilon}\int_{\text{cavity volume}} \boldsymbol{D}_n \cdot \boldsymbol{D}_m \, d\tau$$

$$= \frac{k_n^2 k_m^2 q_n q_m}{2\varepsilon}\int_{\text{cavity volume}} \boldsymbol{\xi}_n \cdot \boldsymbol{\xi}_m \, dt. \tag{8}$$

Here μ and ϵ are, respectively, the permeability and permittivity within the cavity. In general they are functions of position internal to the cavity.

In the case where $n = m$, these field energies have the form of inductive or capacitive stored energies:

$$L_n = \mu k_n^2 \int_{\text{cavity volume}} |\boldsymbol{\eta}_n|^2 \, d\tau \tag{9a}$$

$$S_n = \frac{k_n^4}{\epsilon}\int_{\text{cavity volume}} |\boldsymbol{\xi}_n|^2 \, d\tau \tag{9b}$$

where L_n is the equivalent series inductance and S_n the equivalent series elastance. Combining (9) with the relation between wavenumber and resonant frequency ($k_n = \omega_n\sqrt{\epsilon\mu}$), it can be shown that

$$\omega_n = \sqrt{\frac{S_n}{L_n}}. \tag{10}$$

In the case where $n \neq m$, cross-coupling terms are defined:

$$L_{nm} = \mu k_n k_m \int_{\text{cavity volume}} \boldsymbol{\eta}_n \cdot \boldsymbol{\eta}_m \, d\tau \tag{11a}$$

$$S_{nm} = \frac{k_n^2 k_m^2}{\epsilon}\int_{\text{cavity volume}} \boldsymbol{\xi}_n \cdot \boldsymbol{\xi}_m \, d\tau. \tag{11b}$$

These are energy storage terms which couple energy between two given modes and in general may include surface reactance effects of the niobium.

Series losses in the superconducting niobium surfaces are represented by the dissipation function F [11], given by

$$F = \frac{1}{2}\int_{\text{niobium surface}} R_s |\boldsymbol{H}|^2 \, ds. \tag{12}$$

Here R_s is defined as the surface resistance, which in general is a function of temperature according to the BCS theory [12]–[14]. Combining (12) and (1),

$$F_{nm} = \frac{1}{2}\dot{q}_n \dot{q}_m R_{nm} \tag{13}$$

where

$$R_{nm} = k_n k_m \sqrt{R_{sn} R_{sm}} \int_{\text{niobium surface}} \boldsymbol{\eta}_n \cdot \boldsymbol{\eta}_m \, ds. \tag{14}$$

For a normal conductor the relation $R = \omega L Q^{-1}$ has been generalized [6] to

$$R_{nm} = \frac{\sqrt{\omega_n \omega_m L_n L_m}}{Q_{nm}} \tag{15}$$

where

$$\frac{1}{Q_{nm}}\frac{\sqrt{\delta_n \delta_m}}{2v}\int_{\text{conductor surface}} \boldsymbol{\eta}_n \cdot \boldsymbol{\eta}_m \, ds. \tag{16}$$

Here δ is the penetration depth for the normal conductor. We regard an analogous effective penetration depth for the superconductor. If $n = m$, (16) defines the quality factor associated with niobium losses for an individual mode. However when $n \neq m$ (16) defines a quality factor arising from the two modes interacting or aligning in the niobium surface. This mutual dissipative term describes an energy coupling path between the two modes.

Using $T_{nm} - V_{nm}$ as the Lagrangian, the generalized coupled Lagrange equations [11] with respect to q_n and q_m become

$$\begin{bmatrix} L_n & L_{nm} \\ L_{nm} & L_m \end{bmatrix}\begin{bmatrix} \ddot{q}_n \\ \ddot{q}_m \end{bmatrix} + \begin{bmatrix} R_n & R_{nm} \\ R_{nm} & R_m \end{bmatrix}\begin{bmatrix} \dot{q}_n \\ \dot{q}_m \end{bmatrix} + \begin{bmatrix} S_n & S_{nm} \\ S_{nm} & S_m \end{bmatrix}\begin{bmatrix} q_n \\ q_m \end{bmatrix} = \begin{bmatrix} \Theta_n \\ \Theta_m \end{bmatrix} \tag{17}$$

where Θ_n and Θ_m are the emf's induced in the normal mode meshes by currents in the coupling loop. Assuming the loop to be small enough that the current distribution along the loop is uniform, then, for a loop current of i_0,

$$\Theta_n = L_{0n}\frac{di_0}{dt} \quad \text{and} \quad \Theta_m = L_{0m}\frac{di_0}{dt} \tag{18}$$

where L_{0n} is the mutual inductance between the loop and

normal mode mesh n. Defining the mesh currents $i_n = \dot{q}_n$ and $i_m = \dot{q}_m$ and taking the Fourier transform of (17), one obtains

$$j\omega I_0 \begin{bmatrix} L_{0n} \\ L_{0n} \end{bmatrix} = \begin{bmatrix} j\omega L_n + R_n + \dfrac{S_n}{j\omega} & j\omega L_{nm} + R_{nm} + \dfrac{S_{nm}}{j\omega} \\ j\omega L_{nm} + R_{nm} + \dfrac{S_{nm}}{j\omega} & j\omega L_m + R_m + \dfrac{S_m}{j\omega} \end{bmatrix} \cdot \begin{bmatrix} I_n \\ I_m \end{bmatrix}. \quad (19)$$

The equivalent circuit relating to (19) is illustrated in Fig. 2, where L_0 is the loop inductance, Z_{in} the input impedance, and Z_0 the characteristic line impedance. A standard transformer coupling coefficient arising from the probe coupling to the cavity may then be defined:

$$\kappa_n = \frac{L_{0n}}{\sqrt{L_0 L_n}}. \quad (20)$$

It is also possible to define the following cross-coupling coefficients:

1) Magnetic Field Cross Coupling:

$$\Delta_L = \frac{L_{nm}}{\sqrt{L_n L_m}} = \frac{\int_{\text{cavity volume}} \boldsymbol{\eta}_n \cdot \boldsymbol{\eta}_m \, dt}{\left(\int_{\text{cavity volume}} \boldsymbol{\eta}_n \cdot \boldsymbol{\eta}_n \, dt \cdot \int_{\text{cavity volume}} \boldsymbol{\eta}_m \cdot \boldsymbol{\eta}_m \, dt \right)^{1/2}}, \quad -1 \leqslant \Delta_L \leqslant 1. \quad (21a)$$

2) Electric Field Cross Coupling:

$$\Delta_C = \frac{S_{nm}}{\sqrt{S_n S_m}} = \frac{\int_{\text{cavity volume}} \boldsymbol{\xi}_n \cdot \boldsymbol{\xi}_m \, d\tau}{\left(\int_{\text{cavity volume}} \boldsymbol{\xi}_n \cdot \boldsymbol{\xi}_n \, d\tau \cdot \int_{\text{cavity volume}} \boldsymbol{\xi}_m \cdot \boldsymbol{\xi}_m \, d\tau \right)^{1/2}}, \quad -1 \leqslant \Delta_C \leqslant 1. \quad (21b)$$

3) Dissipative Cross Coupling:

$$\Delta_R = \frac{R_{nm}}{\sqrt{R_n R_m}} = \frac{\sqrt{Q_n Q_m}}{Q_{nm}} = \frac{\int_{\text{niobium surface}} \boldsymbol{\eta}_n \cdot \boldsymbol{\eta}_m \, ds}{\left(\int_{\text{niobium surface}} \boldsymbol{\eta}_n \cdot \boldsymbol{\eta}_n \, ds \cdot \int_{\text{niobium surface}} \boldsymbol{\eta}_m \cdot \boldsymbol{\eta}_m \, ds \right)^{1/2}}, \quad -1 \leqslant \Delta_R \leqslant 1. \quad (21c)$$

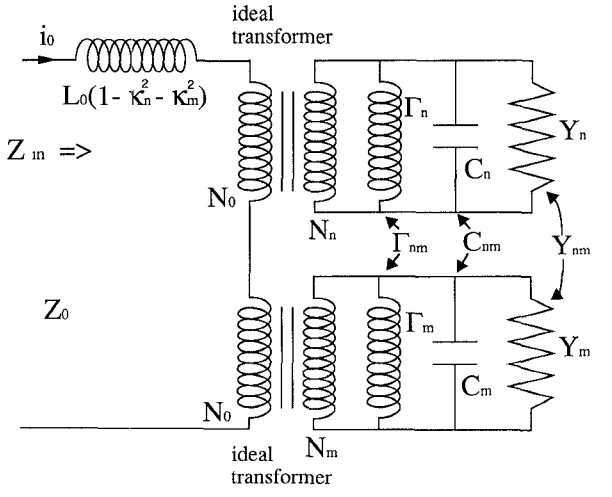

Fig. 3. General equivalent circuit of two excited modes in a loop-coupled dielectric resonator as derived from normal coordinates ϕ_n and ϕ_m.

These coupling coefficients are normalized mutual parameters, which are invariant, regardless of equivalent circuit representation. Thus when we write the equivalent circuit impedance in terms of normalized parameters, we shall write the mutual component in terms of these coupling coefficients.

B. Parallel Circuit Representation of the Sapphire Dielectric

Applying the formalism of subsection A, we shall derive the shunt equivalent circuit of Fig. 3 with respect to the magnetic flux coordinates ϕ_n and ϕ_m. Using (2a) and (2b), the electric and magnetic field energies of two excited modes, n and m, can be represented by the respective Lagrangian variables:

$$T_{nm} = \frac{\epsilon k_n k_m \dot{\phi}_n \dot{\phi}_m}{2} \int_{\text{dielectric volume}} \boldsymbol{\xi}_n \cdot \boldsymbol{\xi}_m \, d\tau \quad (22)$$

$$V_{nm} = \frac{k_n^2 k_m^2 \phi_n \phi_m}{2\mu} \int_{\text{dielectric volume}} \boldsymbol{\eta}_n \cdot \boldsymbol{\eta}_m \, d\tau. \quad (23)$$

These again have the form of energy storage elements as an inductor and a capacitor. In the case where $n = m$,

$$C_n = \epsilon k_n^2 \int_{\text{dielectric volume}} |\boldsymbol{\xi}_n|^2 \, d\tau \quad (24a)$$

$$\Gamma_n = \frac{k_n^4}{\mu} \int_{\text{dielectric volume}} |\boldsymbol{\eta}_n|^2 \, d\tau \quad (24b)$$

where Γ_n is the equivalent parallel reciprocal inductance and C_n is the equivalent parallel capacitance. It follows from (24) and $k_n = \omega_n \sqrt{\epsilon\mu}$:

$$\omega_n = \sqrt{\frac{\Gamma_n}{C_n}}. \quad (25)$$

In the case where $n \neq m$, cross-coupling terms are defined:

$$C_{nm} = \epsilon k_n k_m \int_{\text{dielectric volume}} \boldsymbol{\xi}_n \cdot \boldsymbol{\xi}_m \, d\tau \tag{26a}$$

$$\Gamma_{nm} = \frac{k_n^2 k_m^2}{\mu} \int_{\text{dielectric volume}} \boldsymbol{\eta}_n \cdot \boldsymbol{\eta}_m \, d\tau. \tag{26b}$$

Shunt losses in the cavity dielectric are represented by the dissipation function G, given by

$$G = \frac{1}{2} \int_{\text{dielectric volume}} \sigma_d |E|^2 \, d\tau \tag{27}$$

where σ_d is the dielectric conductivity. The paramagnetic loss associated with chromium impurities has been shown to be negligible [2] and has been omitted. Substituting (2b) into (27) yield

$$G_{nm} = \tfrac{1}{2} \dot{\phi}_n \dot{\phi}_m Y_{nm} \tag{28}$$

where

$$Y_{nm} = k_n k_m \sqrt{\sigma_{d_n} \sigma_{d_m}} \int_{\text{dielectric volume}} \boldsymbol{\xi}_n \cdot \boldsymbol{\xi}_m \, d\tau = \frac{\sqrt{\omega_n \omega_m C_n C_m}}{Q_{nm}} \tag{29}$$

and

$$\frac{1}{Q_{nm}} = \frac{\sqrt{\frac{\epsilon_n''}{\epsilon} \frac{\epsilon_m''}{\epsilon}}}{v_d} \int_{\text{dielectric volume}} \boldsymbol{\xi}_n \cdot \boldsymbol{\xi}_m \, d\tau. \tag{30}$$

Here $\epsilon_n''/\epsilon = \sigma_{d_n}/\epsilon\omega_n$ is the nth mode loss tangent, or ratio of imaginary to real permittivity, in the sapphire dielectric.

Using $T_{nm} - V_{nm}$ as the Lagrangian, and defining $\mathscr{J}_n$ and $\mathscr{J}_m$ as the mmf induced in the normal mode meshes by currents in the coupling loop, the generalized coupled Lagrange equations with respect to ϕ_n and ϕ_m become

$$\begin{bmatrix} C_n & C_{nm} \\ C_{nm} & C_m \end{bmatrix} \begin{bmatrix} \ddot{\phi}_n \\ \ddot{\phi}_m \end{bmatrix} + \begin{bmatrix} Y_n & Y_{nm} \\ Y_{nm} & Y_m \end{bmatrix} \begin{bmatrix} \dot{\phi}_n \\ \dot{\phi}_m \end{bmatrix} + \begin{bmatrix} \Gamma_n & \Gamma_{nm} \\ \Gamma_{nm} & \Gamma_m \end{bmatrix} \begin{bmatrix} \phi_n \\ \phi_m \end{bmatrix} = \begin{bmatrix} \mathscr{J}_n \\ \mathscr{J}_m \end{bmatrix}. \tag{31}$$

Conservation of mmf in each mesh implies that

$$\frac{N_0}{N_n} \mathscr{J}_n = \frac{N_0}{N_m} \mathscr{J}_m = i_0.$$

The effective turns ratio, N_0/N_n, is calculated from the ratio of the primary and secondary magnetizing inductances, $\kappa_n^2 L_0$ and Γ_n^{-1}, respectively, and is given by $N_0/N_n = \sqrt{\kappa_n^2 L_0 \Gamma_n}$. Subtracting the magnetizing inductances from the loop inductance, the overall leakage inductance referred to the primary can be written as $L_0(1 - \kappa_n^2 - \kappa_m^2)$. Expressing (31) in terms of node voltages $V_n = \dot{\phi}_n$ and $V_m = \dot{\phi}_m$, (31) Fourier transforms to

$$I_0 \begin{bmatrix} \frac{N_0}{N_n} \\ \frac{N_0}{N_m} \end{bmatrix} = \begin{bmatrix} j\omega C_n + Y_n + \frac{\Gamma_n}{j\omega} & j\omega C_{nm} + Y_{nm} + \frac{\Gamma_{nm}}{j\omega} \\ j\omega C_{nm} + Y_{nm} + \frac{\Gamma_{nm}}{j\omega} & j\omega C_m + Y_m + \frac{\Gamma_n}{j\omega} \end{bmatrix} \cdot \begin{bmatrix} V_n \\ V_m \end{bmatrix}. \tag{32}$$

This describes the circuit illustrated in Fig. 3 after adding the series leakage inductance.

The parallel cross coupling coefficients are evaluated as follows:

1) Magnetic Field Cross Coupling:

$$\Delta_L = \frac{\Gamma_{nm}}{\sqrt{\Gamma_n \Gamma_m}} = \frac{\int_{\text{dielectric volume}} \boldsymbol{\eta}_n \cdot \boldsymbol{\eta}_m \, d\tau}{\left(\int_{\text{dielectric volume}} \boldsymbol{\eta}_n \cdot \boldsymbol{\eta}_n \, d\tau \cdot \int_{\text{dielectric volume}} \boldsymbol{\eta}_m \cdot \boldsymbol{\eta}_m \, d\tau \right)^{1/2}}, \quad -1 \leq \Delta_L \leq 1. \tag{33a}$$

2) Electric Field Cross Coupling:

$$\Delta_C = \frac{C_{nm}}{\sqrt{C_n C_m}} = \frac{\int_{\text{dielectric volume}} \boldsymbol{\xi}_n \cdot \boldsymbol{\xi}_m \, dt}{\left(\int_{\text{dielectric volume}} \boldsymbol{\xi}_n \cdot \boldsymbol{\xi}_n \, dt \cdot \int_{\text{dielectric volume}} \boldsymbol{\xi}_m \cdot \boldsymbol{\xi}_m \, dt \right)^{1/2}}, \quad -1 \leq \Delta_C \leq 1. \tag{33b}$$

3) Dissipative Cross Coupling:

$$\Delta_R = \frac{Y_{nm}}{\sqrt{Y_n Y_m}} = \frac{\sqrt{Q_n Q_m}}{Q_{nm}} = \frac{\int_{\text{dielectric volume}} \boldsymbol{\xi}_n \cdot \boldsymbol{\xi}_m \, dt}{\left(\int_{\text{dielectric volume}} \boldsymbol{\xi}_n \cdot \boldsymbol{\xi}_n \, d\tau \cdot \int_{\text{dielectric volume}} \boldsymbol{\xi}_m \cdot \boldsymbol{\xi}_m \, d\tau \right)^{1/2}}, \quad -1 \leq \Delta_R \leq 1. \tag{33c}$$

These cross-coupling coefficients are invariant when referred to the primary or secondary coils of the ideal

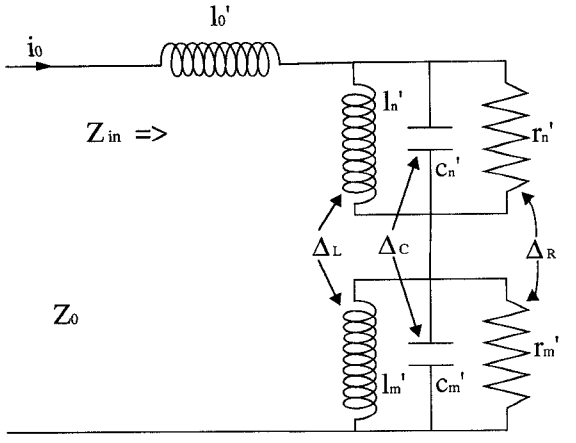

Fig. 4. Both Fig. 2 and Fig. 3 can be represented as a series combination of parallel *LCR* circuits with a defined coupling coefficient between like elements.

transformers in Fig. 3. The mutual capacitance and reciprocal inductance are not invariant. This fact highlights why the former are useful when considering a normalized impedance of the cavity for theoretical purposes.

C. Significance to the Overall T-SLOSC Equivalent Circuit

Deriving the input impedances of Fig. 2 and Fig. 3 gives the same input impedance (Fig. 4), illustrating the duality of the circuits. However the parameters relating to the series circuit involve the niobium superconductor, while the parallel circuit involves the sapphire dielectric. A general circuit as shown in Fig. 4 is considered, where each parameter may have more than one contribution arising from the sapphire and niobium parts internal to the cavity.

The four individual mode circuit elements may be expressed in terms of the four cavity-coupling parameters, $Q_n, L_0, \omega_n, \kappa_n$:

$$l_0' = L_0\left(1-\kappa_n^2-\kappa_m^2\right) \tag{34a}$$

$$r_n' = \kappa_n^2 L_0 \omega_n Q_n \tag{34b}$$

$$l_n' = \kappa_n^2 L_0 \tag{34c}$$

$$c_n' = \frac{1}{\kappa_n^2 L_0 \omega_n^2}. \tag{34d}$$

L_0 and κ_n depend on the probe properties and its placement in the cavity. If the transformer coupling is zero, then the probe does not couple to any modes, and the input impedance is equal to the loop reactance. As the transformer coupling increases, the series reactance diminishes and coupling to the mode increases. Probe stepper motors that work cryogenically are used to adjust penetration into the cavity to vary the coupling. Both the niobium and the sapphire contribute to Q_n by $Q_n^{-1} = Q_{\mathrm{Sapp}\,n}^{-1} + Q_{\mathrm{Nb}\,n}^{-1}$ [15], [2]. For high-Q modes ω_n is dominated by the sapphire dielectric [2], [3] while the niobium cavity perturbs it only very slightly.

For modeling purposes it is convenient to express the input impedance of the circuit in Fig. 4 in terms of the normalized parameters $\beta_n = r_n'/Z_0$, $\alpha = l_0'\omega_n/Z_0$, $y_n = (\omega-\omega_n)/\omega_n$, and Q_n and the cross-coupling coefficients from either (21) or (33). Thus it can be shown that

$$\frac{Z_{\mathrm{in}}}{Z_0} = \frac{\beta_n\Lambda_n + \beta_m\Lambda_m - 2\sqrt{\beta_n\beta_m}\,\Lambda_n\Lambda_m B_{nm}}{1-\Lambda_n\Lambda_m B_{nm}^2} + j\alpha \tag{35}$$

where

$$\Lambda_n = \frac{1}{1+2jQ_n y_n}$$

is a Lorentzian of unity coupling and

$$B_{nm} = \Delta_R + j\sqrt{Q_nQ_m}\left(\Delta_C\left((y_n+1)(y_m+1)\right)^{1/2} - \Delta_L\left((y_n+1)(y_m+1)\right)^{-1/2}\right)$$

is a mutual cross term arising from the derived cross-coupling coefficients. The reflection coefficient is defined by

$$\rho = \frac{\frac{Z_{\mathrm{in}}}{Z_0}-1}{\frac{Z_{\mathrm{in}}}{Z_0}+1} = \frac{\beta_n\Lambda_n + \beta_m\Lambda_m - 2\sqrt{\beta_n\beta_m}\,\Lambda_n\Lambda_m B_{nm} + (j\alpha-1)\left(1-\Lambda_n\Lambda_m B_{nm}^2\right)}{\beta_n\Lambda_n + \beta_m\Lambda_m - 2\sqrt{\beta_n\beta_m}\,\Lambda_n\Lambda_m B_{nm} + (j\alpha+1)\left(1-\Lambda_n\Lambda_m B_{nm}^2\right)}. \tag{36}$$

By expressing both mode frequencies in terms of a tuning parameter and graphing the reflection coefficient at various tunings, the behavior of closely tuned modes can be investigated. Mathematica allows the algebra to be handled with ease.

III. Observations of Coupled Modes

The model describing coupled mode behavior was tested using the apparatus shown schematically in Fig. 5. The sapphire resonator has two unperturbed high-Q modes at 10.439 and 10.22 GHz; both occur in doublet pairs. Experimental tuning curves for one of each pair of doublets are shown in Fig. 6. The tuning variable x is measured in millimeters from the top of the sapphire resonator to the tuning disk. A decrease in the observed Q of each mode occurs when a low-Q mode is tuned close to the high-Q mode under investigation.

Q degradation for the 10.439 GHz modes was observed for x between 7 and 8 mm. The effect was seen on three

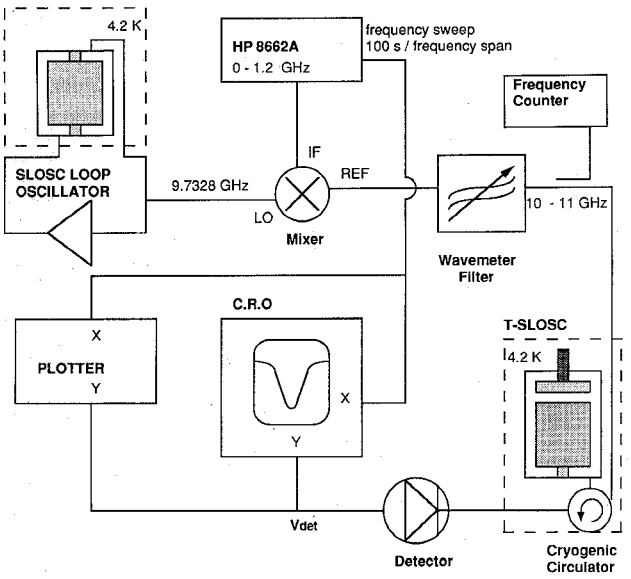

Fig. 5. An ultrastable swept microwave frequency source is obtained by mixing a fixed-frequency SLOSC oscillator with an HP 8662A synthesizer locked to a frequency standard. The resultant signal is then swept slowly over the T-SLOSC in reflection, at 100 s per frequency span. The voltage V_{det} is measured from the detector in the range where it is proportional to $|\rho|^2$. From this plot, Q and coupling can be measured.

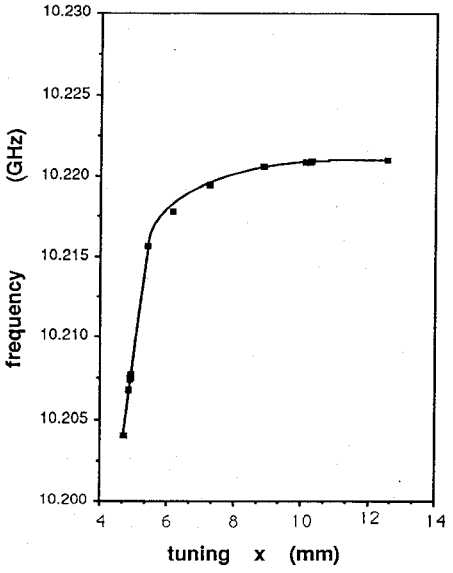

Fig. 6. Mode frequency and unloaded Q curves versus tuning for one of each of the 10.22 GHz and 10.439 GHz high-Q doublet pairs. Unloaded Q curves are directly beneath the corresponding frequency curves.

experimental runs and has never been observed for the 10.22 GHz mode. Since the field patterns are not known in detail, one can only postulate why this occurs. Either the niobium tuning stem links a significant fraction of the field, creating additional dissipation, or there is a reactive coupling to some distant mode. This would require larger coupling coefficients than those presently measured (see next section).

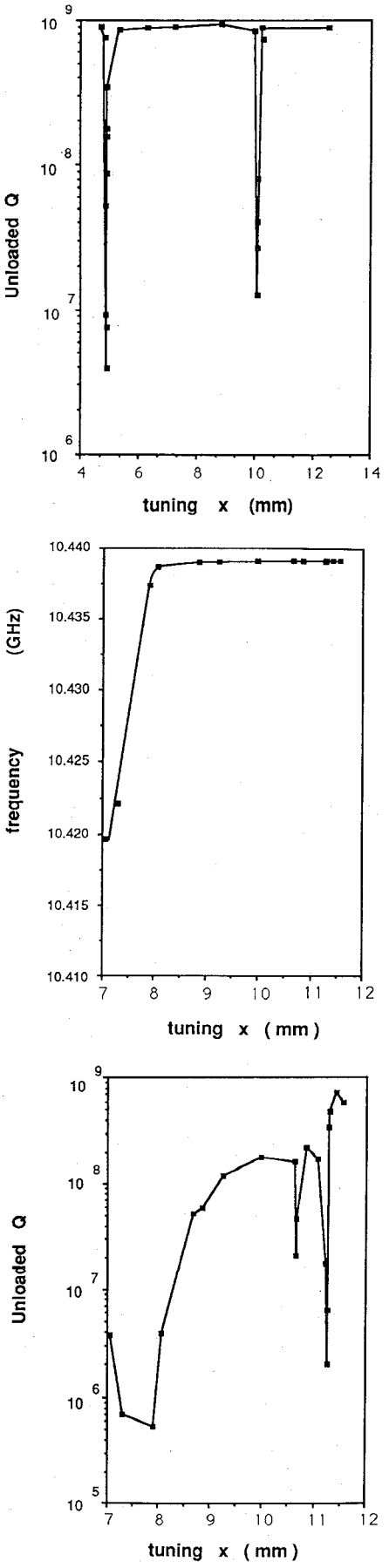

Fig. 6. (*Continued*)

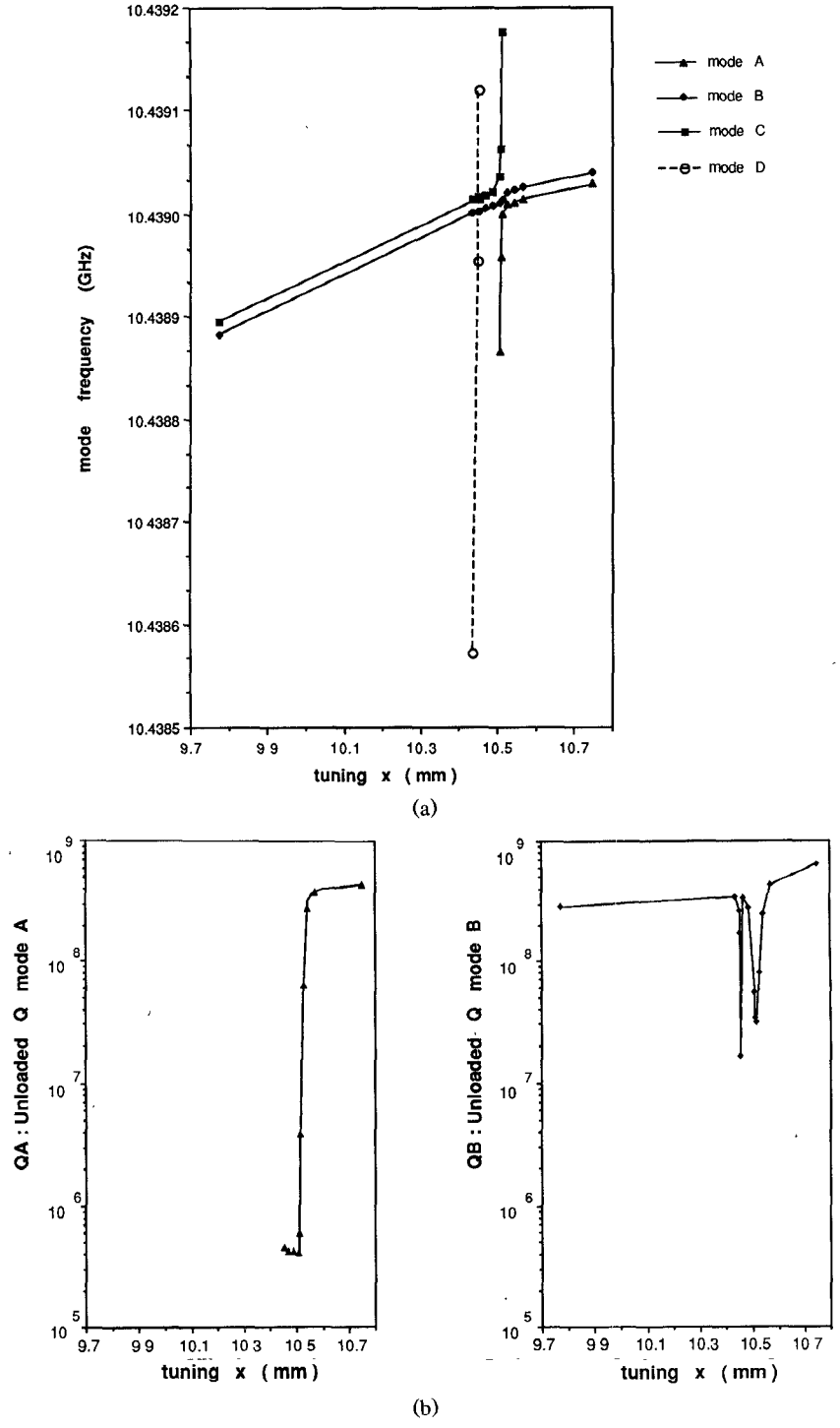

Fig. 7. The interaction of a low-Q doublet pair with the 10.439 GHz doublet pair. (a) Frequency versus tuning curves during the interaction. (b) Unloaded Q variations of each mode during the interaction. (*Continued on next page.*)

Fig. 6(b) (10.439 GHz) was plotted using a room-temperature circulator rather than the cryogenic circular shown in Fig. 5. The 1.5 m of coaxial cable leading out of the cryogenic Dewar greatly enhanced line resonances. Section V shows that line resonances affect cavity resonances through a resistive interaction between the probes. To measure cavity properties, a line resonance can be detuned away from cavity resonances by varying a line stretcher between the room-temperature circulator and the T-SLOSC. After the addition of the cryogenic circulator, the interaction around $x = 10.2$ mm was observed with greater accuracy, shown in Fig. 7.

IV. Reactive Coupling

For reactive coupling (ignoring damping), the method of Goldstein [11] calculates the resonant frequencies from $\det(V_{nm} - \omega^2 T_{nm}) = 0$. Using circuit elements of Fig. 5,

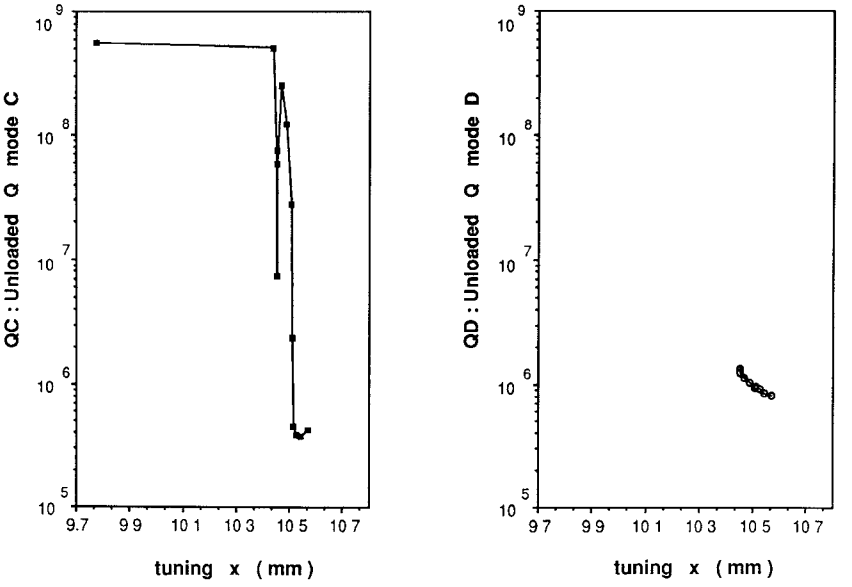

Fig. 7. (b) (*Continued*)

we obtain

$$\det\begin{pmatrix} \frac{1}{l'_n} - \omega^2 c'_n & \frac{1}{l'_{nm}} - \omega^2 c'_{nm} \\ \frac{1}{l'_{nm}} - \omega^2 c'_{nm} & \frac{1}{l'_m} - \omega^2 c'_m \end{pmatrix} = 0 \qquad (37)$$

or

$$\omega^4(1-\Delta_C) + \omega^2\left(2\Delta_C\Delta_L\omega_n\omega_m - \omega_n^2 - \omega_m^2\right) + (1-\Delta_L)\omega_n^2\omega_m^2 = 0.$$

It is assumed that the interacting modes have linear tuning coefficients, so $\omega_n = \omega_0(1 + \Delta x'/2)$ and $\omega_m = \omega_0(1 - \Delta x'/2)$, where $\Delta x'$ is an arbitrary dimensionless tuning unit. The solution to first order in $\Delta x'$ and $\Delta_L - \Delta_C$ is

$$\omega_{1,2} = \omega_0\left(1 \pm \frac{\sqrt{\Delta x'^2 + (\Delta_L - \Delta_C)^2}}{2}\right). \qquad (38)$$

This shows that the two modes always have a minimum frequency separation when $\Delta x' = 0$, owing to the reactive coupling between the two modes.

Experimentally, it is possible to measure the net reactive coupling by

$$|\Delta_T| = |\Delta_L - \Delta_C| = \left.\frac{\omega_1 - \omega_2}{\omega_0}\right|_{\Delta x' = 0}. \qquad (39)$$

Equations (21) and (33) allow couplings of either sign. Negative inductive coupling has the same effect as positive capacitive coupling; thus it is impossible to determine experimentally whether the coupling is through the magnetic or the electric field. However, the reactive coupling can be measured and substituted into Mathematica for simulation. The interaction is not symmetrical, so the coupling coefficient sign can be determined by comparing the simulation with experiment.

A general interaction of two doublet pairs requires four mode equivalent circuits, with cross-coupling elements between each mode circuit. For the higher frequency interaction illustrated in Figs. 7 and 8, the dominant coupling occurs between mode A and mode C. Mode D is too far away in frequency, while mode B only couples very weakly in this interaction. This is highlighted by Q_B dropping an order of magnitude less than Q_A and mode B's tuning curve deviating only slightly, while mode A and mode C swap characteristics. Thus the model derived for two interacting modes should be applicable.

The linear tuning curve for modes A and C in the vicinity of the interaction are measured and found to be (from Fig. 7)

$$f_A = f_0[1.0281\ 10^{-5}\Delta x + 1]$$
$$f_C = f_0[5.4276\ 10^{-3}\Delta x + 1]. \qquad (40)$$

The frequency of intersection between the two lines in (40) is given by $f_0 = 10.43900$ GHz, and Δx is given by $\Delta x = x - x_0$, where $x_0 = 10.5107$ mm. High precision in relative values of x is achieved by a stepper motor, although the systematic error in the absolute value is much greater owing to the possibility of thermal differential movement during cooling.

Before the interaction the following parameters were measured (assuming $\alpha = 0$): $Q_A = 10^8$, $Q_C = 4 \cdot 10^5$, $\beta_A = 2$, and $\beta_C = 0.7$. Using (41) the mutual coupling is estimated from the experimental curve in Fig. 8(b) to be; $\Delta_T = -1.0 \cdot 10^{-5}$. This is an overestimate since $x \neq x_0$. After a few trials $\Delta_T = -8.5 \cdot 10^{-6}$ gives a reasonable agreement with experiment. Experimental and theoretical curves are compared in Fig. 8.

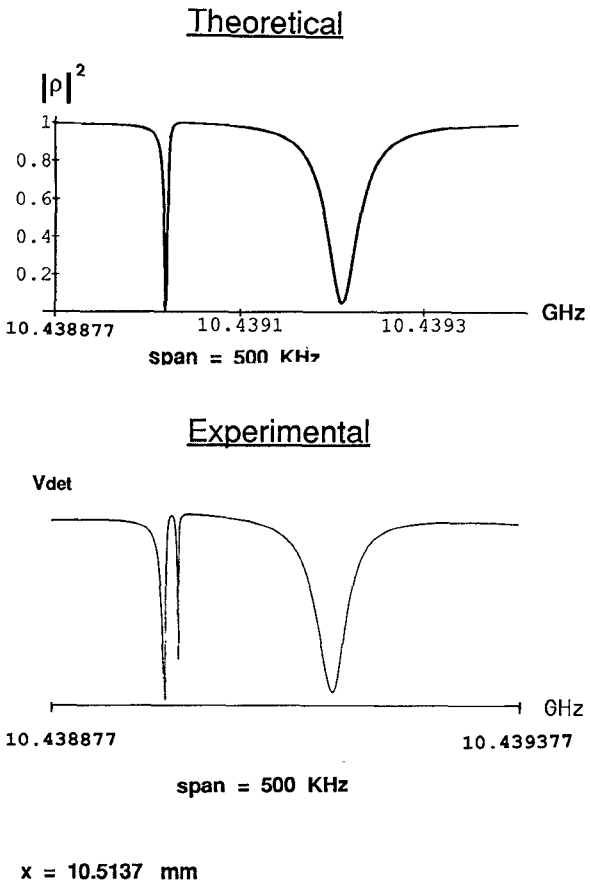

(a)

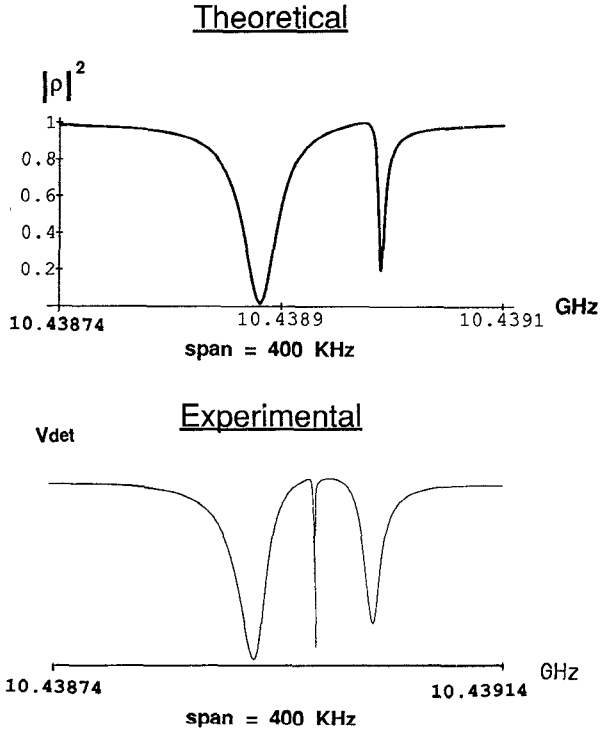

(b)

Fig. 8. The higher frequency interaction from Fig. 7 with the experimentally observed interaction compared with a theoretical simulation.

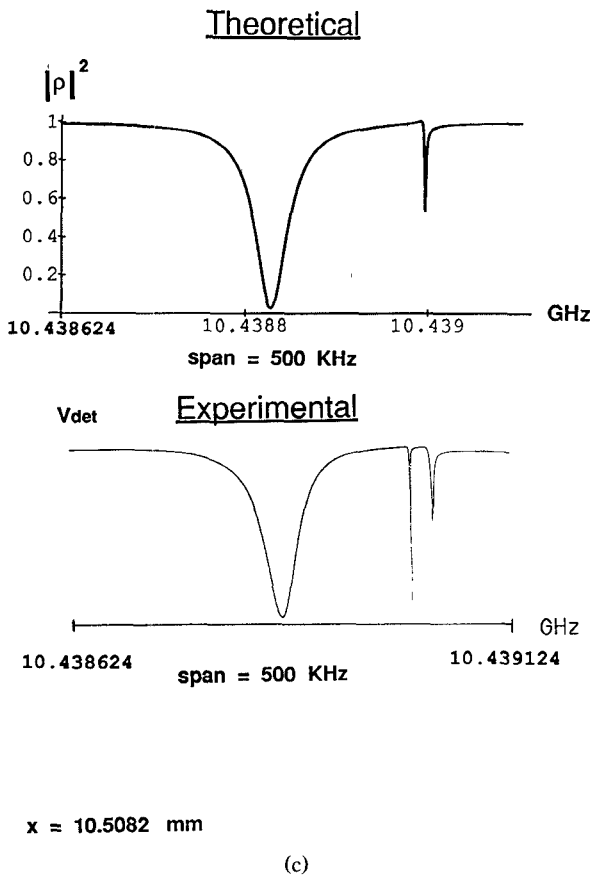

(c)

Fig. 8. (*Continued*)

The lower frequency interaction in Fig. 7 is more complicated, as modes B and C interact simultaneously with mode D to about the same order of magnitude. The mutual coupling is estimated from (39) to give $\Delta_T \approx -2 \cdot 10^{-6}$. This smaller coupling enables the high-Q modes to get closer to the bandwidth of the low-Q mode. For the 10.22 GHz mode interactions, cross-coupling coefficients are of the order of $-5 \cdot 10^{-5}$.

The mechanism of this reactive coupling is either via the electric field, as one might expect in a dielectric resonator, or via the magnetic field through a chromium electron spin resonance. This chromium resonance has been observed to cause a power-dependent coupling between modes in a fixed-frequency SLOSC [16], which causes frequency pulling of one mode when power is injected into another. It is possible that this coupling is another manifestation of this effect.

V. Resistive Coupling

Resistive couplings were observed between line resonances and most cavity resonances before the cryogenic circulator was added to the circuit in Fig. 5. The line resonances had Q factors of about $5.5 \cdot 10^2$ with varying couplings. After adding the cryogenic circulator, the effects of line resonances were negligible, owing to the

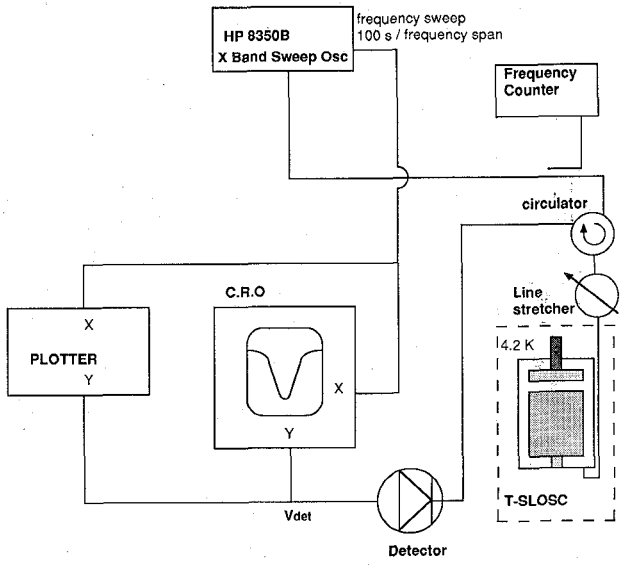

Fig. 9. An HP 8350B is used to span over a line resonance so interactions with a T-SLOSC resonance can be observed. The line stretcher is used to frequency pull the line resonances.

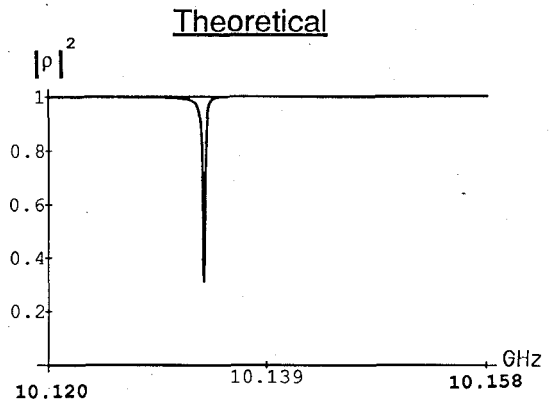

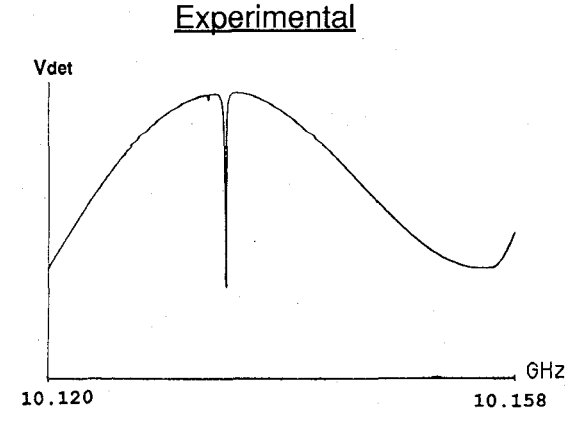

(a)

Fig. 10. The experimental effects and theoretical simulation of frequency pulling a line resonance across a T-SLOSC resonant mode.

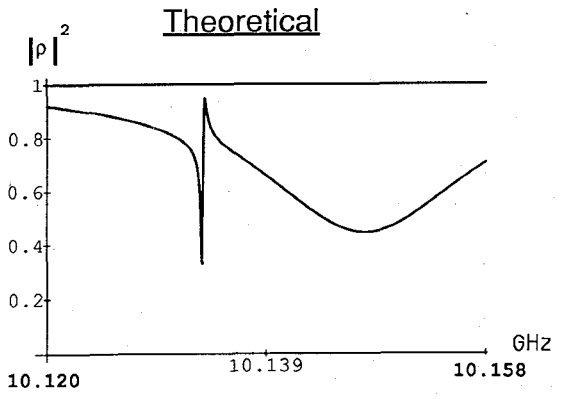

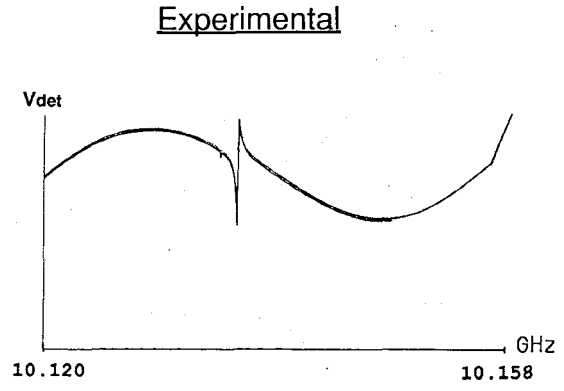

(b)

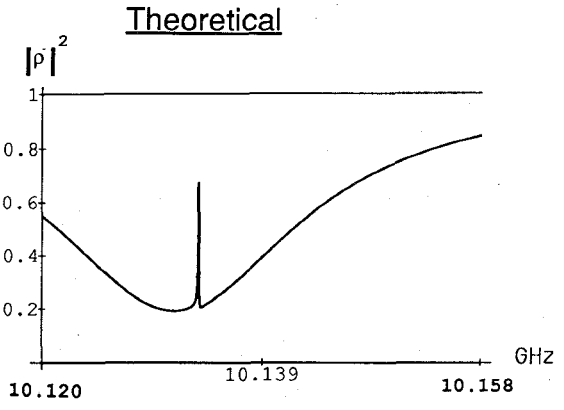

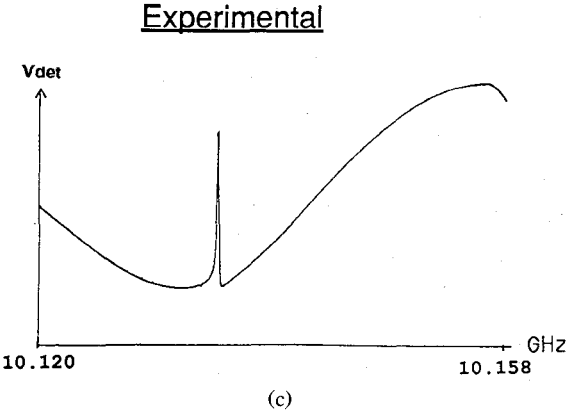

(c)

Fig. 10. (*Continued*)

reduction of the line length and the number of connectors from the probe to the circulator.

The circuit in Fig. 5 cannot span the bandwidth of a line resonance because of the wavemeter in the circuit. Thus the circuit in Fig. 9 was used to observe a line resonance interact with a mode of $Q \approx 10^5$ and $\beta \approx 3.5$. An overcoupled mode is observed because from (36) it is apparent that mutual effects will be enhanced for an overcoupled mode. The frequency stability of the microwave sweeper allowed the study only of low-Q modes with this circuit; however the same effects on high-Q modes were observed using the circuit of Fig. 5 with a room-temperature circulator. The line stretcher in Fig. 9 was used to frequency pull a line resonance across the T-SLOSC mode under investigation. Fig. 10 shows a comparison between experiment and theory.

Line resonances couple to cavity resonances through a niobium loop probe. From (21c),

$$\Delta_R = \frac{\int_{\text{niobium probe}} \boldsymbol{\eta}_n \cdot \boldsymbol{\eta}_m \, ds}{\left(\int_{\text{niobium probe}} \boldsymbol{\eta}_n \cdot \boldsymbol{\eta}_n \, ds \int_{\text{niobium probe}} \boldsymbol{\eta}_m \cdot \boldsymbol{\eta}_m \, ds \right)^{1/2}}.$$

The value $\Delta_R = 0.9$ was found to give good agreement between the model and experiment (Fig. 10). The cavity resonance distorts as it tunes across the line resonance.

VI. Conclusion

Interactions between various modes in a tunable sapphire-loaded superconducting cavity have been studied. The main features that emerge are as follows:

1) Reactive coupling causes modes to influence each other beyond their bandwidths, because in (38) the reactive factor in B_{nm} is multiplied by the geometric mean of Q_n and Q_m.
2) Reactively coupled modes do not tune across each other; they become hybrids of each other and eventually change identities. The reactive cross coupling can be calculated by the closest point of tuning between the two modes.
3) Resistively coupled modes influence each other only if one can be tuned in the bandwidth of another.
4) To measure the T-SLOSC mode properties among a line resonance, the line resonance must be tuned away by a line stretcher, so that the line resonance does not affect the cavity resonance through a mutual resistance in the probe.

This paper has successfully modeled some of the complex phenomena that occur in a tunable multimode cavity. In spite of the complex interactions, Q factors greater than 10^8 can be achieved, with a useful tuning range of the order of tens of MHz. This technology provides a means of creating ultra-low-phase-noise microwave sources, with applications in radar, space tracking, radio astronomy, and other areas of high-precision metrology.

Acknowledgment

The authors are grateful to A. J. Giles, S. K. Jones, and P. J. Veitch for their invaluable advice and assistance in the laboratory. They also thank P. J. Turner for his critical comments of the submitted manuscript.

References

[1] P. J. Veitch, D. G. Blair, N. P. Linthorne, L. D. Mann, and D. K. Ramm, "Development of a 1.5-tonne niobium gravitational radiational antenna," *Rev. Sci. Instr.*, vol. 58, no. 10, Oct. 1987.
[2] S. K. Jones, "Frequency stabilization with a sapphire loaded superconducting cavity," Ph.D. thesis, Dept. Physics, University of Western Australia, 1988.
[3] A. J. Giles, S. K. Jones, D. G. Blair, and M. J. Buckingham, "A high stability microwave oscillator based on a sapphire loaded superconducting cavity," in *Proc. IEEE 43rd Annual Freq. Contr. Symp.*, 1989, pp. 89–93.
[4] D. G. Blair and A. M. Sanson, "High Q tunable sapphire loaded cavity resonator for cryogenic operation," *Cryogenics*, vol. 29, Nov. 1989.
[5] M. E. Tobar and A. G. Mann, "Resonant frequencies of higher order modes in cylindrical anisotropic dielectric resonators," in *IEEE MTT-S Int. Microwave Symp. Dig.*, June 1991, pp. 143–146.
[6] C. G. Montgomery, R. H. Dicke, and E. M. Purcell, *Principles of Microwave Circuits* (M.I.T. Radiation Laboratory Series). New York: McGraw-Hill, 1948.
[7] A. Baños, Jr. "Theory of ringing time of tunable echo boxes," Radiation Laboratory M.I.T., Report 630, Nov. 3, 1944.
[8] V. F. Vzyatyshev and G. P. Rayevskiy, "Interaction effects of azimuthal oscillations in dielectric disk resonators," *Radiotekhnika i elektronika*, no. 4, pp. 877–878, 1987.
[9] P. D. Crout, "An extension of lagrange's equations to electromagnetic field problems; equivalent networks," Radiation Laboratory M.I.T., Report 628, Oct. 6, 1944.
[10] S. Wolfram, *Mathematica: A System for Doing Mathematics by Computer*. Reading, MA: Addison-Wesley, 1988.
[11] H. Goldstein, *Classical Mechanics*. Reading, MA: Addison-Wesley, 1959.
[12] J. Bardeen, L. N. Cooper and J. R. Schrieffer, "Theory of superconductivity," *Phys. Rev.*, vol. 108, no. 5, pp. 1175–1204, 1957.
[13] J. P. Turneaure and I. Weissman, "Microwave surface resistance of superconducting niobium," *J. Appl. Phys.*, vol. 39, no. 9, pp. 4417–4427, 1968.
[14] V. B. Braginsky and V. I. Panov, "Superconducting resonators on sapphire," *IEEE Trans. Magn.* vol. MAG-15, pp. 30–32, Jan. 1979.
[15] J. C. Slater, *Microwave Electronics*. New York: Van Nostrand, 1950.
[16] A. J. Giles, "Electron spin resonance phenomena in a sapphire loaded superconducting cavity oscillator," Ph.D. thesis, Dept. Physics, University of Western Australia, 1991.

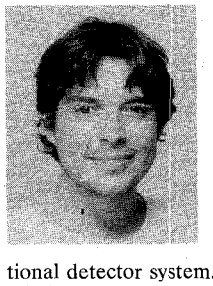

Michael E. Tobar (S'87) was born in Maffra, Australia, on January 3, 1964. He received the B.Sc. degree in theoretical physics and mathematics in 1985 and the B.E. (hons) degree in electrical and computer systems engineering in 1988 from Monash University, Melbourne, Australia. In 1989 he began work for the Ph.D. degree with the gravitational radiation research group at the University of Western Australia. He is now investigating the low-noise requirements of a transducer in a gravitational radiational detector system.

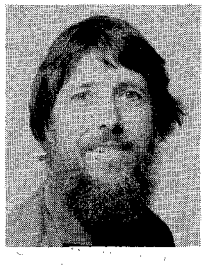

David G. Blair was born in Hampshire, England, on November 26, 1946. He received the B.Sc. (hons) degree in physics from the University of Western Australia in 1967. In 1972 he received the Ph.D. degree from the University of East Anglia, England. His dissertation was entitled "Superflow: A Study of Superfluid Helium Films."

From 1972 to 1973 he was a Science Research Associate at the University of East Anglia. His research included design of high-vacuum, optical, cryogenic, and superconducting apparatus. From 1973 to 1976 he was a Visiting Assistant Professor at Louisiana State University. He worked on the construction of a pair of large-scale cryogenic gravitational radiation antennas, where he developed an ultrasensitive position transducer using thin-film niobium on sapphire superconducting resonators. Since 1976 he has been with the University of Western Australia, where he is now a Senior Lecturer in the Department of Physics. He is chief supervisor and initiator of the Gravitational Radiation Research Project at the University of Western Australia. His research projects have included acoustic losses in niobium; superconducting magnetically levitated systems; supernovas, black holes, and neutron stars; and ultra-low-noise microwave electronic systems.

Dr. Blair has authored approximated 90 papers throughout his career in the above research areas.